ACS Catalysis

pubs.acs.org/acscatalysis

Research Article

Controlling the Competition: Boosting Laccase/HBT-Catalyzed Cleavage of a β-O-4′ Linked Lignin Model

Roelant Hilgers, Annemieke van Dam, Han Zuilhof, Jean-Paul Vincken, and Mirjam A. Kabel*

Cite This: ACS Catal. 2020, 10, 8650−8659

Read Online

ACCESS | Metrics & More | Article Recommendations | Supporting Information

ABSTRACT: Over the past years, laccase/mediator systems (LMS) have received a lot of attention as potential sustainable tools for biocatalytic lignin degradation. Nevertheless, it has often been reported that C_α-oxidation, rather than ether bond cleavage, is the main result of LMS treatments, which limits the overall efficiency and effectiveness. Remarkably few studies have attempted to influence this product profile and thereby enhance the effectivity of LMS-catalyzed lignin degradation. Here, we studied the influence of buffer properties on the product profile of a β-O-4′ linked lignin model dimer upon conversion by a laccase/hydroxybenzotriazole system. We show that the ratio between β-O-4′ ether cleavage and C_α-oxidation can be substantially increased by using unconventional buffer properties (i.e., highly concentrated buffers at near-neutral pH). Whereas <10% ether cleavage was obtained in conventional buffer (i.e., weak buffer at pH 4), as much as 80% ether cleavage was obtained in highly concentrated buffers at pH 6. In addition, this alteration of buffer properties was found to improve the stability of both laccase and mediator. The underlying reactions were further studied by using experimental and computational (density functional theory, DFT) approaches. Based on the outcomes, we propose detailed reaction mechanisms for the reactions underlying ether cleavage and C_α-oxidation. We propose that increasing buffer pH or increasing buffer strength enhances H-bonding between the lignin model and buffer anions, which drives the overall reaction outcome toward ether cleavage. These insights may pave the way for more efficient and effective biocatalytic lignin degradation.

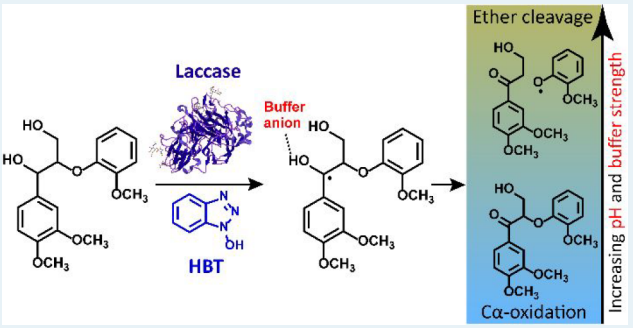

KEYWORDS: *lignocellulose, biocatalysis, reaction mechanisms, mediator, density functional theory, H-bonds, competition*

INTRODUCTION

Lignin is a highly abundant aromatic polymer in plant cell walls, and its selective degradation is a major challenge in biorefinery. Lignin mainly consists of syringyl (S), guaiacyl (G), and *p*-hydroxyphenyl (H) units, coupled via a variety of interunit linkages, of which the β-O-4′ linkage is most abundant (45−94% of the total interunit linkages).[1] The polymer consists of phenolic subunits (10−30%), mainly being the end-caps of the polymer, and nonphenolic subunits (70−90%), forming the backbone.[2] Although lignin can be degraded by using thermochemical treatments, green alternatives are preferred and are receiving increasing attention.

A potential green approach for selective lignin degradation is the use of laccase/mediator systems (LMS). Laccases (EC 1.10.3.2) are oxidases with redox potentials of <800 mV[1] that use molecular oxygen to perform one-electron oxidations of aromatic substrates. Laccases can oxidize the phenolic lignin subunits, which have sufficiently low redox potentials, but oxidation of the nonphenolic subunits having redox potentials up to 1500 mV is hampered.[3] To overcome the inertness of nonphenolic subunits, a mediator can be added to form a LMS. In such a system, laccase oxidizes the mediator, which subsequently oxidizes the nonphenolic lignin structure. The most widely used mediator is 1-hydroxybenzotriazole (HBT). Other commonly used mediators are TEMPO ((2,2,6,6-tetramethylpiperidin-1-yl)oxyl) and ABTS (2,2′-azino-bis(3-ethylbenzothiazoline-6-sulfonic acid)).

These mediators oxidize lignin substructures via different mechanisms. For TEMPO, an ionic mechanism has been proposed.[4] ABTS has been suggested to operate via electron transfer (ET), although this has not been unambiguously demonstrated.[5] HBT is generally assumed to oxidize nonphenolic lignin structures via hydrogen atom transfer (HAT),[5,6] although it has been suggested that electron transfer (ET) may also occur in the case of relatively electron-rich lignin substructures.[7] Oxidation of lignin substructures via HAT and ET results in the formation of benzylic radicals and

Received: May 15, 2020
Revised: July 10, 2020
Published: July 10, 2020

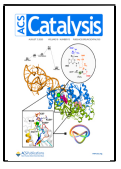

https://dx.doi.org/10.1021/acscatal.0c02154
ACS Catal. 2020, 10, 8650−8659

radical cations, respectively. These radicals react further (nonenzymatically) via several routes, depending on the structure of the substrate.[8−12] Studies on LMS treatments of nonphenolic β-O-4′ linked lignin model compounds mainly report C_α-oxidation[13] and bond cleavage as outcomes,[10−12,14,15] and it has been suggested that their formation occurs via competing routes.[1,10] Typically, C_α-oxidation is the major reaction outcome, whereas cleavage products are only formed in minor amounts.[12,14,15] Obviously, when LMS treatments are performed with the aim to degrade lignin, this product distribution is undesirable and should be shifted in favor of bond cleavage.

In principle, to increase the efficiency of LMS-catalyzed lignin degradation, two strategies could be followed: (i) maximizing the total extent of oxidation by increasing the catalytic performance of the LMS or (ii) steering the nonenzymatic follow-up reactions toward bond cleavage (at the cost of C_α-oxidation). Whereas multiple studies have been published related to the catalytic performance of different laccases and mediators (in line with the first approach),[16−20] to the best of our knowledge, no studies have been published that follow the second approach. In addition, as LMS treatments are often performed at those conditions under which the laccase is optimally active, it is largely unknown whether and how reaction conditions can affect the reaction product profile.

Here, we show that altering buffer pH and buffer strength can dramatically enhance degradation of a nonphenolic lignin model, veratrylglycerol-β-guaiacyl ether (VBG), by a laccase/HBT system. Furthermore, based on additional experiments and a computational (DFT) study, we provide new insights into the competition between C_α-oxidation and ether bond cleavage and the underlying mechanisms.

MATERIALS AND METHODS

Materials. Veratrylglycerol-β-guaiacyl ether (VBG) was purchased from ABCR (Karlsruhe, Germany). Laccase from *Trametes versicolor*, HBT, ABTS, and all other chemicals were purchased from Sigma-Aldrich (St. Louis, MO, U.S.A.). The laccase was partially purified as described previously.[21] Water was prepared by using a Milli-Q water purification system (Merck Millipore, Billerica, MA).

Buffers Used in This Study. In this study, citrate/phosphate buffers were used at various pH values and buffer strengths. In this article, a X/Y mM citrate/phosphate buffer refers to a buffer prepared from X mM citric acid and Y mM dibasic phosphate stock solutions. It should be noted that the actual concentrations of citrate and phosphate are pH dependent.

Laccase Activity Determination. Laccase activity was determined spectrophotometrically by oxidation of ABTS (1 U = 1 μmol ABTS oxidized per minute at pH 5). The partially purified laccase had a specific activity of approximately 50 U/mg.

Incubation of VBG with the Laccase/HBT System. *Incubations at Varying pH Values.* Stock solutions of 0.2 mM VBG, 1 mM HBT, and 10 U/mL laccase were prepared in MQ water. Citrate/phosphate buffers were prepared at pH 3, 4, 5, 6, and 7 by mixing 50 mM citric acid and 100 mM dibasic sodium phosphate at different ratios. VBG, HBT, laccase and buffer were then mixed in a ratio of 1:1:1:2, to obtain final concentrations of 0.04 mM VBG, 0.2 mM HBT, 2 U/mL laccase and 20/40 mM citrate/phosphate buffer. It should be noted that relatively high mediator concentrations were used in this study, with the purpose to speed up conversion of VBG. All samples were prepared in duplicate. The mixtures were incubated at 40 °C and 400 rpm in a thermomixer (Eppendorf, Hamburg, Germany). After 2, 6, 24, and 48 h, 40 μL of the incubation mixture was collected and 10 μL of 20 mM sodium azide was added to the aliquots to stop the reaction. The samples were centrifuged (10 000*g*, 5 min, 20 °C) and analyzed by using RP-UHPLC-PDA-MS^n. Calibration curves of VBG (5−50 μM), and the main reaction products CLP (0.2−20 μM) and VBG_{ox} (1−40 μM) (see section: large-scale preparation and purification of reaction products) were prepared in triplicate, and were included in the RP-UHPLC-PDA-MS analysis to quantify VBG, VBG_{ox}, and CLP after incubation. To estimate the formed quantities of the reaction product CLP II, the calibration curve of CLP was used. From these calibration curves, the extinction coefficients of CLP and VBG_{ox} relative to that of VBG were determined. In further experiments, only calibration curves of VBG were included, and quantities of CLP and VBG_{ox} were calculated based on their relative molar absorption coefficients.

Incubations at Varying Buffer Strengths. Samples were prepared according to the procedure described above, with final citrate/phosphate buffer concentrations of 5/10, 20/40, 40/80, and 80/160 mM (citrate/phosphate) and incubated for 48 h. Similarly, incubations were performed in MQ water instead of buffer. The pH of these incubation mixtures was adjusted to 4 or 6 by addition of HCl and NaOH. During incubation, the pH change of these samples was less than 0.15 pH point. Incubations (48 h) in concentrated citrate buffers (only at pH 4 and 6) were performed with a final citrate concentrations of 2 M and a laccase activity of 4 U/mL. For comparison, incubations (48 h) in a 20/40 mM citrate/phosphate buffer were performed with an equal laccase dose (i.e., 4 U/mL).

Large-Scale Production and Purification of Reaction Products. To enable quantification of the main reaction products, a large-scale incubation of VBG with laccase/HBT was performed, after which the reaction products were purified. Hereto, two batches of 50 mg of VBG and 125 mg of HBT were incubated in 40 mL of citrate/phosphate buffers (20/40 mM) at pH 4 and 6. Laccase was added to obtain a final activity of 10 U/mL. After 48 h, the reaction mixtures were centrifuged (5000*g*, 20 °C, 10 min) and the reaction products were separated using flash chromatography. Hereto, the centrifuged reaction mixtures were injected on a Reveleris Flash system (Grace Davison Discovery Sciences, Columbia, MD, USA), equipped with a 4 g Reveleris RP Flash cartridge, ELSD detector and UV detector. The eluents used were water (eluent A) and ACN (eluent B), both containing 1% (v/v) formic acid. After activation of the cartridge with eluent B, and washing with 5 column volumes of eluent A, the reaction mixtures were injected. The reaction products and remaining VBG were then separated using the following elution profile: 0−5 min at 0% B (isocratic), 5−33 min from 0 to 32% B (linear gradient), 33−33.6 min from 32 to 100% B (linear gradient), and 33.6−36 min at 100% B (isocratic). The flow was set at 18 mL/min and fractions of 4 mL were collected. The resulting fractions were diluted 10 times with water and analyzed by using RP-UHPLC-PDA-MS. Fractions that contained the reaction products and that were free of byproducts were pooled. The remaining ACN was evaporated under reduced pressure, after which the model compound solutions were freeze-dried and stored in a desiccator.

https://dx.doi.org/10.1021/acscatal.0c02154
ACS Catal. 2020, 10, 8650−8659

The fractions containing pure CLP or VBG_{ox} were pooled and freeze-dried. The obtained CLP and VBG_{ox} were analyzed using RP-UHPLC-PDA-MS and 2D NMR (HSQC, HMBC, and COSY) to confirm purity and identity of the products. Since no completely pure fractions of CLP II could be obtained, the most pure fraction was freeze-dried and analyzed using HSQC and HMBC NMR.

2D NMR Analysis. The purified reaction products were analyzed by using 2D NMR. Hereto, VBG_{ox} (490 μg), CLP (360 μg), and CLP II (300 μg, partly purified) were dissolved in 450 μL of DMSO-*d*, after which the solutions were transferred to Shigemi NMR tubes. The NMR experiments were recorded at 25 °C by using hsqcetgpsisp2.2 and hmbcgpndqf pulse sequences on a Bruker AVANCE III 600 MHz NMR spectrometer (Bruker BioSpin, Rheinstetten, Germany) equipped with a 5 mm cryo-probe. For VBG_{ox} and CLP, a cosygpqf pulse sequence was used as well. The internal temperature of the probe was set at 298 K. The solvent peak (DMSO-d_6) was used as an internal reference (δ_C 39.5 ppm; δ_H 2.49 ppm). Data acquisition and processing was performed by using Topspin 4.0.1 (Bruker).

RP-UHPLC-PDA-MS Analysis. Analysis of reaction mixtures were performed using a Vanquish UHPLC system (Thermo Scientific, San Jose, CA, U.S.A.) coupled to a PDA detector and either a Thermo LTQ Velos Pro ion-trap mass spectrometer or a Thermo Q Exactive Focus hybrid quadrupole-orbitrap mass spectrometer. Previously reported methods were used for both UHPLC-PDA-MS systems,[15] with the only adaptation being the elution profile: 0−1.5 min at 5% B (isocratic), 1.5−28 min from 5 to 35% B (linear gradient), 28−28.8 min from 35 to 100% B (linear gradient), 28.8−33.3 min at 100% B (isocratic), 33.3−34 min from 100 to 5% B (linear gradient), and 34−38 min at 5% B (isocratic).

Preparation of C_α-Deuterated VBG ($VBG_{C\alpha\text{-}D}$). For the preparation of C_α-deuterated VBG, purified VBG_{ox} was used as starting material. Hereto, 2 mg of VBG_{ox} was dissolved in 2 mL of 5% methanol, and approximately 1 mg of $NaBD_4$ was added. The mixture was left at room temperature for 1 h, after which the C_α-deuterated VBG ($VBG_{C\alpha\text{-}D}$) was extracted three times with 0.5 mL of diethyl ether. The diethyl ether was evaporated under a continuous flow of N_2, and $VBG_{C\alpha\text{-}D}$ was dissolved in 5% methanol. The purity was checked by using RP-UHPLC-PDA-MS. A single peak was observed with m/z 358, corresponding to the $[M + Na]^+$ ion of $VBG_{C\alpha\text{-}D}$. No remaining VBG_{ox}, nondeuterated VBG or other impurities were observed. The deuterated VBG was freeze-dried and stored in a desiccator until further use.

Determination of Kinetic Isotope Effects. Kinetic isotope effects (KIE) were determined at pH 3, 4, 5, and 6 by performing intermolecular competition experiments. Hereto, VBG and $VBG_{C\alpha\text{-}D}$ were incubated for 48 h with the laccase/HBT system, starting with equimolar concentrations of 0.04 mM (see section "Incubation of VBG with the Laccase/HBT System: Incubations at Varying pH Values" for details). The KIE was then determined by quantification of VBG and $VBG_{C\alpha\text{-}D}$ using high resolution RP-UHPLC-PDA-MS.

Computational Analyses. All quantum chemical calculations were performed with the B97D functional and 6-311+G(d,p) basis set, as implemented in Gaussian 16 (version B1), using a SMD solvent model for water.[22]

RESULTS AND DISCUSSION

Conversion of VBG by the Laccase/HBT System. Incubations of VBG with laccase/HBT were performed in citrate/phosphate buffers at pH 3−7. In all cases, three reaction products were detected: The C_α-ketone analogue of VBG (VBG_{ox}) and two ether cleavage products (CLP and CLP II; Figures 1 and 2; see Table S1 and Figure S1−3 for UHPLC-MS and NMR based identification). VBG_{ox} was found to be the major product, which is in line with previous findings in the literature.[12,14,15]

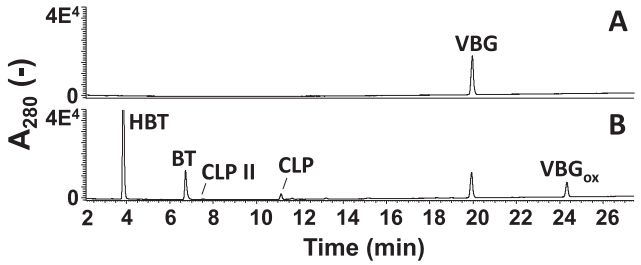

Figure 1. RP-UHPLC-UV_{280} chromatograms of VBG (A) and VBG incubated for 48 h with laccase/HBT in a 20/40 mM citrate/phosphate buffer at pH 6 (B). BT = benzotriazole. Chromatograms of incubations at other pH values and incubations times and data used for product identification can be found in the Supporting Information.

During the incubation, HBT was partly converted to benzotriazole (BT) (23−86% based on UV peak ratio, Table S2). It should be noted that, upon formation of CLP and CLP II, other cleavage products should have been formed as well (i.e., products containing the other aromatic ring of VBG). These products were not detected, most likely because they reacted further to multiple other products.

Effect of pH and Buffer Strength on Product Distribution. Laccase/HBT incubations performed at pH 3−7 in 20/40 mM citrate/phosphate buffers were followed over time (Figure S4). Regarding the extent of VBG conversion, pH 4 and 5 were found to be the optimum pH values, showing 45 and 54% conversion, respectively, after 48 h (Figure 3).

The relatively high conversion may justify why most lignin and lignin model compound incubations in literature are performed at these, for the laccase more optimal, pH values.[11,12,23−27] Nevertheless, the pH was shown to strongly affect the product distribution. At pH 3 and 4, mainly VBG_{ox} was formed and the cleavage products were only formed to a minor extent (i.e., both <6% of the reaction products). At higher pH values, the product distribution shifted in favor of the cleavage products, mainly due to an increased formation of CLP (Figure 3). At pH 6 and 7, the cleavage products together accounted for 38% of the reaction products. The product ratios did not show a strong dependence on incubation time (data not shown). Regarding absolute amounts, the optimal pH for cleavage of VBG was pH 6, due to a higher laccase activity at pH 6 than at pH 7. The formation of CLP II was highest at low pH values, but rather low yields (≤1%) were found in all incubations, indicating that cleavage of the *O*-4′ bond occurs only to a very limited extent. Therefore, in further investigations, we focused on the formation of VBG_{ox} and CLP.

Although it seemed that the pH influenced the reaction product profile, it is important to note that by increasing the

https://dx.doi.org/10.1021/acscatal.0c02154
ACS Catal. 2020, 10, 8650−8659

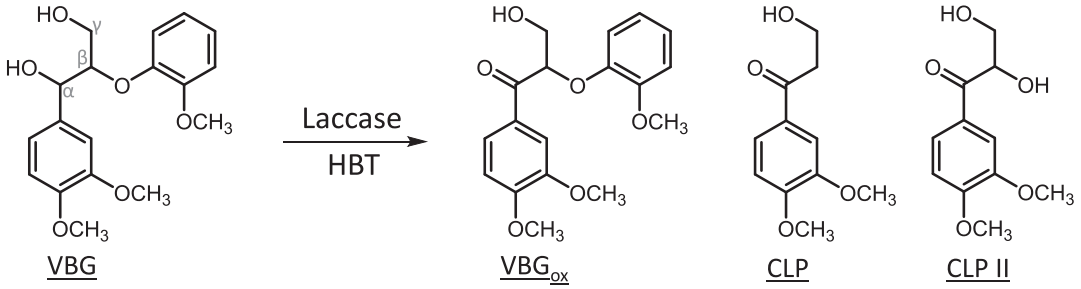

Figure 2. Reaction products of VBG formed upon incubation with the laccase/HBT system. Identification of the reaction products was based on RP-UHPLC-PDA-MS and NMR (see the Supporting Information).

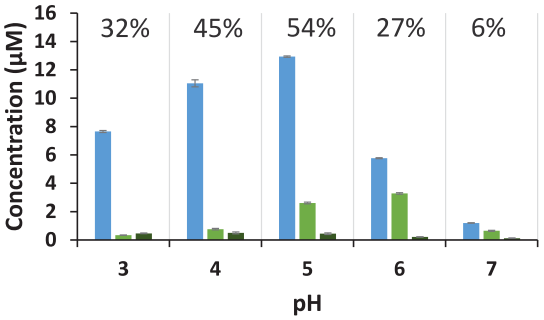

Figure 3. Molar concentration of the reaction products VBG_{ox} (blue), CLP (green), and CLP II (dark green) after incubation with laccase/HBT for 48 h in 20/40 mM citrate/phosphate buffers. Percentages refer to the conversion of VBG. The error bars represent the standard deviation of two independent incubations.

buffer pH, also the phosphate/citrate ratio and the dissociation of citrate and phosphate increased. Therefore, we investigated whether the observed differences in product ratios (see Figure 3) were effects of pH or (also) of the concentration of specific ions. Hereto, the incubations of VBG were repeated in 5/10 mM, 40/80 mM and 80/160 mM citrate/phosphate buffers. Interestingly, the molar ratio CLP/VBG_{ox} was found to increase not only with increasing pH but also with increasing buffer strength (Figure 4). In absence of a buffer, a pH effect was still observed, although the ratio CLP/VBG_{ox} was significantly lower than in buffered incubations. These results indicate that the product ratio is not determined by a "simple"

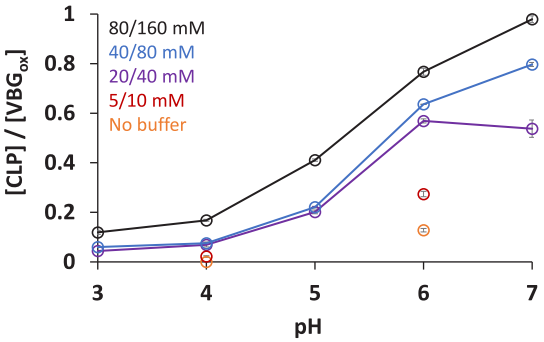

Figure 4. Molar ratios between CLP and VBG_{ox} after incubation of VBG for 48 h with laccase/HBT in buffers prepared from 5/10 mM (red), 20/40 mM (purple), 40/80 mM (blue), and 80/160 mM citrate/phosphate (black) or nonbuffered solutions of which the pH was adjusted using NaOH and HCl (yellow). The error bars represent the standard deviation of two independent incubations.

pH dependence but that the ratio CLP/VBG_{ox} is considerably affected by the presence of buffer ions.

Based on the insights described above, we attempted to further enhance ether cleavage of VBG by performing incubations in highly concentrated (2 M) citrate buffers at pH 4 and 6. After 48 h, 34−40% of the VBG was converted, and CLP/VBG_{ox} ratios as high as 0.9 and 3.9 were obtained at pH 4 and 6, respectively (Figure 5).

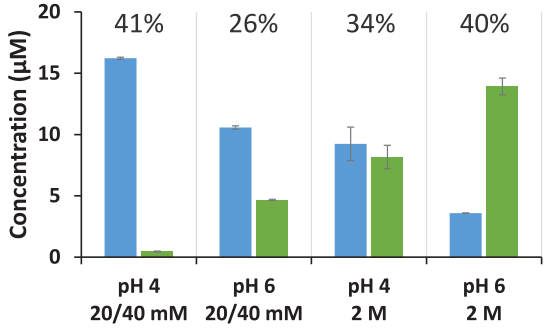

Figure 5. Molar concentrations of the reactions products VBG_{ox} (blue) and CLP (green) after incubation of VBG with laccase/HBT in 20/40 mM citrate/phosphate or 2 M citrate buffers for 48 h. Percentages refer to the conversion of VBG. The error bars represent the standard deviation of two independent incubations.

The latter ratio is 138 times higher than that obtained in the control experiment (20/40 mM citrate/phosphate buffer at pH 4), and demonstrates the enormous impact of the buffer properties on the reaction outcome. Interestingly, after 48 h of incubation, the residual laccase activity was larger in the concentrated citrate buffers than in the weak citrate/phosphate buffers, and substantially less HBT was degraded to BT (Table S2). Hence, the increased extent of ether bond cleavage does not occur at the cost of enzyme stability.

Experimental Insights into the Effect of Reaction Conditions on Product Distribution. *Competing or Sequential Formation of VBG_{ox} and CLP?* Our next step was to understand in more detail how the buffer properties affect the product distribution in laccase/HBT incubations. First, we verified that the two dominant reaction products (i.e., VBG_{ox} and CLP) are true end products of the incubation, and that they are formed through competing, rather than sequential reactions. To this aim, purified VBG_{ox} and CLP were incubated with laccase/HBT at pH 4 and 6. After 24 h, no conversion was found for both products, confirming that both VBG_{ox} and CLP are end products of the laccase/HBT treatment, formed via competing reaction pathways (Figure S5).

https://dx.doi.org/10.1021/acscatal.0c02154
ACS Catal. 2020, 10, 8650−8659

Role of Laccase Activity. As the results shown in Figure 3 were obtained from incubations with the same amount (and not activity) of laccase at all pH values, we checked whether the observed pH effects were caused indirectly by the effect of pH on laccase activity toward HBT. Although laccase loading slightly affected the ratio CLP/VBG_{ox} (Figure S6), the differences were too small to explain the results shown in Figure 3. Based on these verifications, it was concluded that CLP and VBG_{ox} should be formed from laccase-independent, competing reactions.

Buffer or Salt Effects in the Competing Reactions? The ratio CLP/VBG_{ox} was found to increase with increasing pH and buffer strength. As both buffer strength and pH are positively correlated with ionic strength, due to increased concentration and dissociation of ions, respectively, we investigated whether the ratio CLP/VBG_{ox} could also be enhanced by increasing the ionic strength with a nonbuffer salt (i.e., KNO_3). As can be observed from Figure 6, the addition of

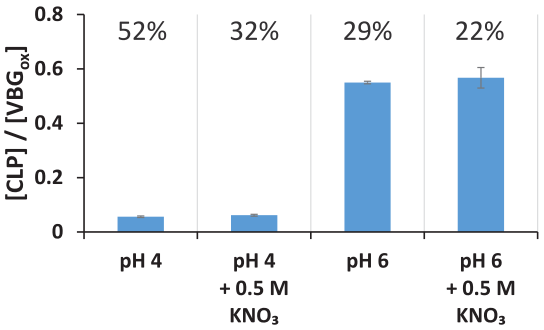

Figure 6. Molar product ratios (CLP/VBG_{ox}) after incubation of VBG for 48 h with laccase/HBT in buffers at pH 4 and 6 prepared from 20/40 mM citrate/phosphate, and in the same buffers supplemented with 0.5 M KNO_3. The error bars represent the standard deviation of two independent incubations. The percentages refer to the conversion of VBG.

0.5 M KNO_3 did not significantly affect the product ratio. From this, it can be inferred that the product ratio is not affected by the ionic strength of the reaction medium but rather by the concentration of specific buffer ions.

Do Buffer pH and Strength Affect the Oxidation Mechanism? To define the exact starting point of the observed competition reactions, we investigated whether oxidation of VBG by the HBT radical would result in the formation of benzylic radicals (via HAT) and/or radical cations (via ET). Although it is generally assumed that the laccase/HBT system operates via a HAT mechanism, evidence for this has only been obtained by using monomeric lignin model substrates and only at pH 5.[5,28] In another study, in which a dimeric lignin model was used, it has been suggested that laccase/HBT can operate via both HAT and ET.[7] We, therefore, investigated whether a HAT or an ET mechanism would be more plausible in the case of VBG oxidation and whether a shift in oxidation mechanism could occur when changing the buffer pH. To this end, we determined the kinetic isotope effect (KIE) of VBG and its C_α-deuterated analogue ($VBG_{C\alpha\text{-}D}$) in intermolecular competition experiments in 20/40 mM citrate/phosphate buffers at pH 3, 4, 5, and 6 (see Figure 7).

In case of a HAT mechanism, a substantial primary KIE can be expected, as cleavage of the C_α-H/D bond occurs at the rate-limiting step. In contrast, no substantial KIE is expected in the case of ET, as the C_α-H/D bond is not involved in the rate-limiting step.[5] Relatively large KIEs (4.1−6.3) were found for all pH values (Table 1).

Table 1. Kinetic Isotope Effects Obtained from an Intermolecular Competition between Oxidation of VBG and C_α-Deuterated VBG ($VBG_{C\alpha\text{-}D}$) upon Incubation with Laccase/HBT for 48 h[a]

pH	KIE (H/D)
3	5.1 ± 0.7
4	5.1 ± 0.3
5	6.3
6	4.1 ± 0.5

[a]Averages and standard deviations of two independent incubations are shown.

As these KIE values clearly point into the direction of a HAT mechanism, and as no clear increasing or decreasing trend in KIE was observed with increasing pH, a shift in oxidation mechanism seems implausible. Thus, we concluded that the competition between CLP and VBG_{ox} formation starts after formation of a VBG benzylic radical.

Computational Insights into the Competing Reaction Mechanisms. To gain further insights into the competing reactions of the VBG benzylic radical, we zoomed in on the reaction mechanisms underlying C_α-oxidation and C_β-O' ether cleavage. Mechanisms have been suggested for both reactions, although few efforts have been made to provide evidence for these mechanisms.[7,30] To check the plausibility of the suggested mechanisms and to obtain more insights into the structures of the transition states (TS) and intermediates, we

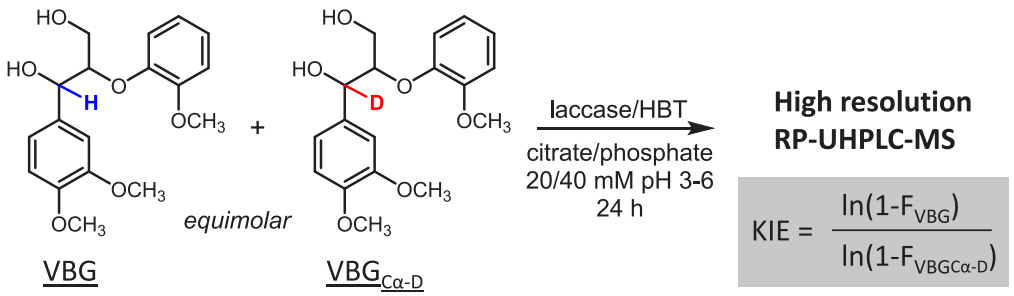

Figure 7. Schematic overview of the kinetic isotope effect (KIE) determination. The KIE was determined by comparing conversion rates of VBG and its C_α-deuterated analogue $VBG_{C\alpha\text{-}D}$ in an intermolecular competition experiment. The KIE was then determined by using the formula shown in the figure, wherein F = fraction of substrate converted.[29]

https://dx.doi.org/10.1021/acscatal.0c02154
ACS Catal. 2020, 10, 8650−8659

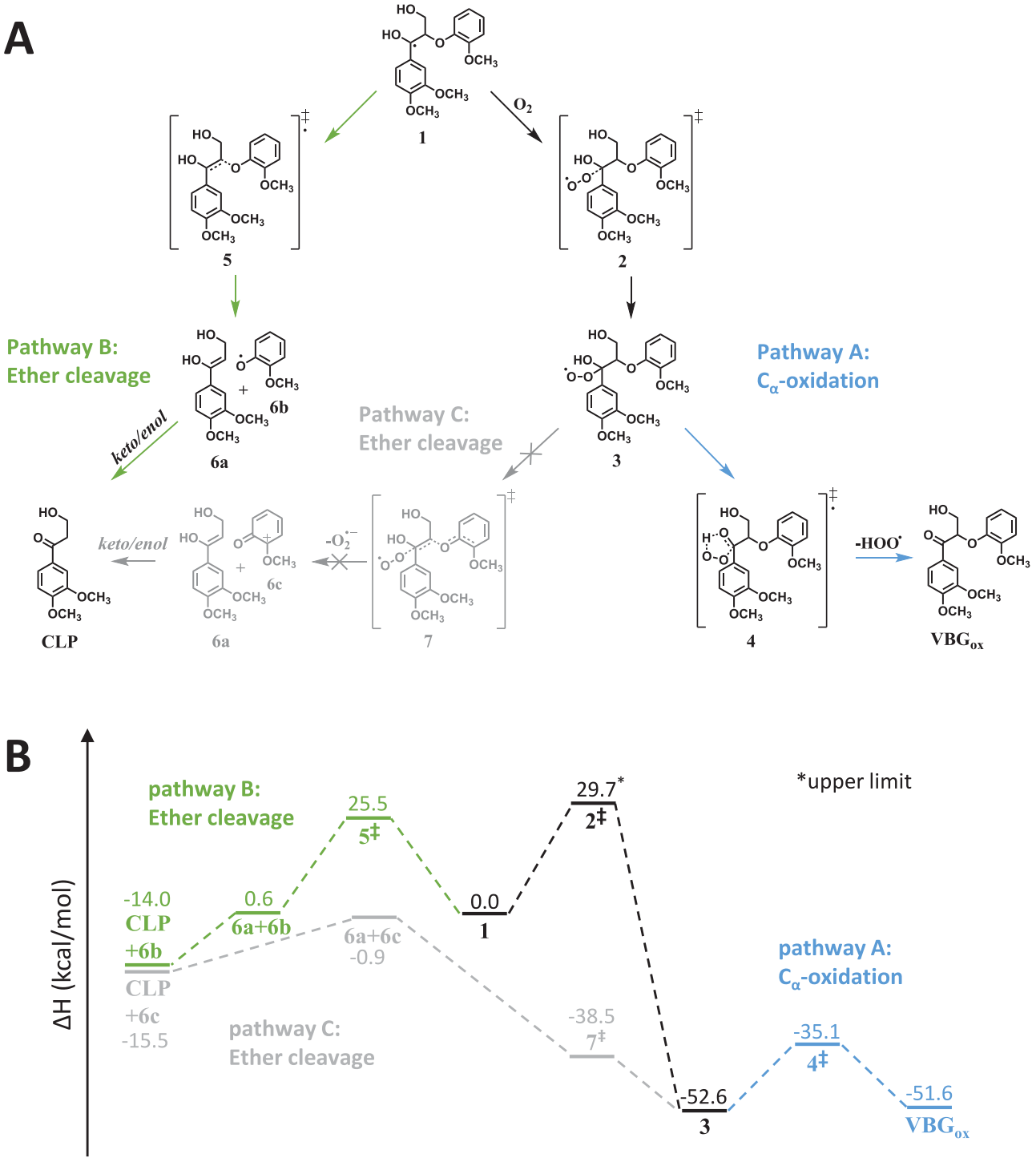

Figure 8. Proposed reaction mechanisms in the literature (panel A) for C_α-oxidation (pathway A) and C_β-O' cleavage (pathways B and C) of the VBG benzylic radical, with calculated relative enthalpies of intermediates, transition states, and products (panel B). As structure 6b and 6c rapidly react further, the final relative enthalpies of the cleavage pathways (B and C) are expected to be significantly lower than the presented values. Based on the calculations, pathway B is a more plausible cleavage mechanisms than pathway C (gray). * This enthalpy should be interpreted as an upper limit.

performed a Density Functional Theory (DFT) study to determine the relative enthalpies of all structures involved.

C_α-Oxidation. For C_α-oxidation, a mechanism has been suggested in literature that involves addition of O_2 to the benzylic radical, after which the C_α-ketone is formed by splitting off a hydroperoxyl radical (Figure 8, pathway A).[7,30] As the energy-minimized starting point of this step (i.e., structure 1 + O_2) has quartet spin, while the resulting peroxyl radical intermediate (structure 3) has doublet spin, TS 2 is likely to have a blended spin state. We, therefore, started out by potential energy scans assuming either quartet spin (coming from structure 1 and O_2) or doublet spin (coming from structure 3). The quartet-state trajectory yielded a clear TS upon specific geometric restrictions (see Figure S7), while the

https://dx.doi.org/10.1021/acscatal.0c02154
ACS Catal. 2020, 10, 8650−8659

doublet trajectory did not yield a TS. Since the quartet trajectory was higher in energy than the doublet one, this was analyzed in detail, so as to obtain an upper limit to the TS energy. The resulting (quartet) TS structure (Figure S7 and Table S3) has a relative energy of 29.7 kcal/mol compared to the starting materials. As O_2 addition is overall exothermic by 52.6 kcal/mol, it was concluded that O_2 addition is irreversible. The second step of pathway A involves splitting off a hydroperoxyl radical. For this step, a clear TS (structure 4) containing a five-membered ring was found, indicating that the hydroperoxyl radical leaving group is formed through intramolecular H-transfer. The activation energy of this second step equals 17.5 kcal/mol. Thus, depending on how much doublet spin character is involved in TS 2, the activation energy of pathway A is predicted to be in the range of 17.5−29.7 kcal/mol. Although the calculated enthalpy gain of splitting of a hydroperoxyl radical is essentially zero, the reaction is probably driven forward by entropy gain and/or further reactions of the hydroperoxyl radical.

C_β-O′ Ether Cleavage. For C_β-O′ ether cleavage, two different mechanisms have been reported in literature. The first mechanism involves a homolytic cleavage of the C_β-O′ bond directly from the benzylic radical (Figure 8, pathway B), whereas the second mechanism involves O_2 addition followed by heterolytic cleavage of the C_β-O′ bond (Figure 8, pathway C).[7,30]

In pathway B, the relative enthalpy of the TS for the C_β-O′ bond cleavage was calculated to be 25.5 kcal/mol (structure 5). As the subsequent keto−enol tautomerization is expected to be very fast, and thus not rate-limiting,[31] no further TS was calculated. The overall activation energy of pathway B, thus, equals 25.5 kcal/mol. Although the calculated enthalpy gain of pathway B only equals 14.0 kcal/mol, it should be noted that the formed guaiacol radical (structure 6b) rapidly reacts further, which is expected to further decrease the relative enthalpy of its products. Based on the overall energy gain, and a surmountable activation energy, pathway B seems to be a plausible route.

Pathway C has a slightly higher overall energy gain than pathway B. However, the intermediate after splitting off the superoxide (structure 6c) lies 51.5 kcal/mol higher than its precursor (structure 3), making this pathway unlikely to occur.

Toward an Explanation for the Buffer-Dependent Competition. Based on the DFT study, a competition between pathway A and pathway B seems possible. However, based on the reactions shown in Figure 8, it is not directly clear how this competition would be influenced by the buffer pH and/or strength. Theoretically, as O_2 solubility decreases at high salt levels,[32] pathway A could be slowed down at increased buffer strength and pH. Nevertheless, no significant effects of buffer salts on O_2 solubility are expected in weak buffers, nor did we find any significant differences in O_2 concentrations between buffers at pH 3 and 7 using Oxygraph measurements (data not shown). In addition, if the O_2 solubility would have been the main reason underlying the observed buffer effects, it would be expected that also high concentrations of other salts would affect the product profile. As can be clearly observed from Figure 6, this was not the case.

Since it was found that only buffer ions, and not KNO_3, affected the product ratio, a more plausible scenario is that specific buffer ions interact with the lignin model during the course of the reaction, and thereby influence the competition between ether cleavage and C_α-oxidation. Interestingly, based on the pK_a equalization principle,[33] strong H-bonding can be expected between the secondary alcohol proton in structure 1 and 3 and the citrate trianion or phosphate dianion (see the Supporting Information for a detailed explanation). As the concentrations of these anions increase with increasing pH (in the used pH range) and buffer strength, it is plausible that these anions are indeed involved in the observed buffer effect. Furthermore, by performing DFT calculations, we investigated whether H-bonding between the VBG benzylic radical (structure 1) and citrate would be more favorable for the citrate trianion than for the dianion. Although, in both cases such intermolecular H-bonding would require disruption of the intramolecular H-bond between the C_α−OH and C_γ−OH groups of structure 1, we found that H-bonding between structure 1 and the citrate trianion is favorable by 3.9 kcal/mol (Figure 9).

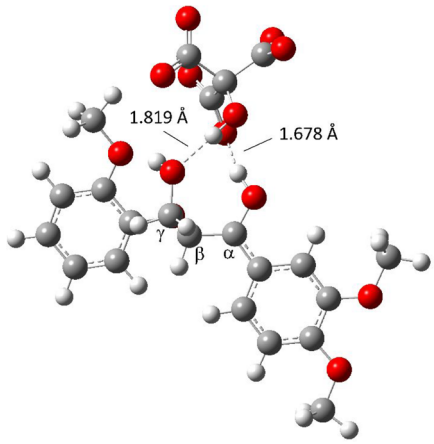

Figure 9. Optimized geometry of the VBG benzylic radical (structure 1) and the citrate^{3-}. The molecules are linked via two H-bonds: one between the C_α−OH proton of the VBG radical and a citrate carboxylate group (bond length = 1.678 Å), and one between the C_γ−OH oxygen and the tertiary alcohol proton of citrate (bond length = 1.819 Å). The overall enthalpy gain obtained by H-bonding is 3.9 kcal/mol. In case of citrate^{2-}, H-bonding to structure 1 is enthalpically unfavorable by 1.9 kcal/mol. It should be noted that the O atom of the aryl-ether is present but largely hidden behind the C_γ-atom.

In contrast, for the citrate dianion, it is unfavorable by 1.9 kcal/mol, i.e., in that case the intramolecular H-bond would be preferred (data not shown). This finding strengthens our suggestion that only specific anions are involved in H-bonding to the lignin model. Two scenarios can be described via which such H-bonding between anions and lignin could affect the observed competition (Figure 10).

First, it has been shown that the rate of O_2 addition to (benzylic) radicals can be substantially diminished by e.g. steric or electronic stabilization of the radical.[34,35] As H-bonding of buffer anions to the secondary alcohol proton brings the anions in close proximity of the radical-bearing carbon atom (Figure 9), and this it is not inconceivable that such H-bonding somehow increases the stability of the radical and thereby decreases the rate of O_2 addition. A lower O_2 addition rate would slow down pathway A but not pathway B, resulting in relatively more ether cleavage (Figure 10A). As there is currently no good model to predict O_2 addition rates to radicals, it remains to be investigated whether H-bonding between buffer anions and lignin radicals indeed slows down O_2 addition.

https://dx.doi.org/10.1021/acscatal.0c02154
ACS Catal. 2020, 10, 8650−8659

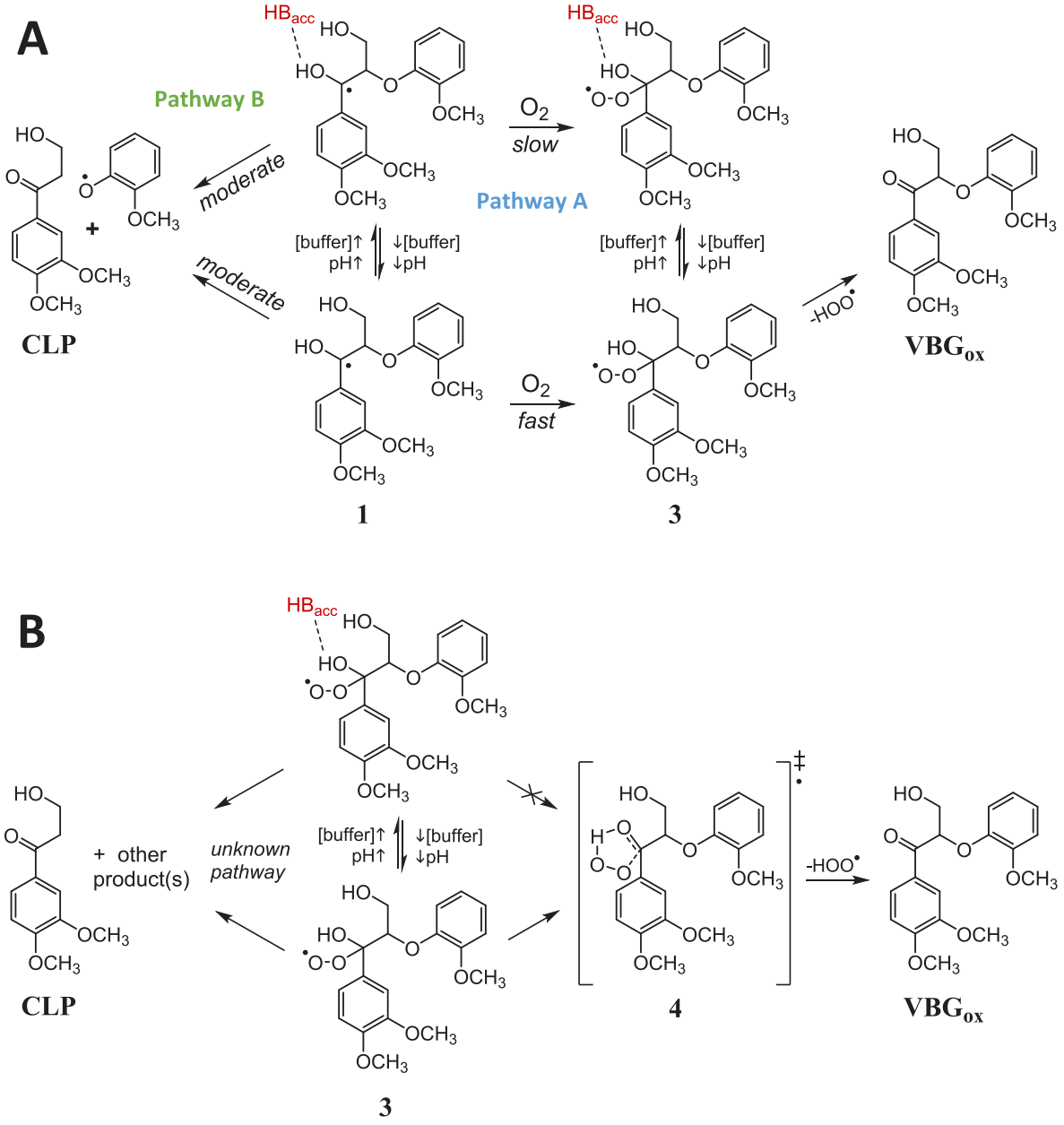

Figure 10. Two possible scenarios for the effect of H-bonding on the competition between C_β-O' ether cleavage and C_α-oxidation. H-bonding between VBG benzylic radicals and buffer anions may slow down the rate of O_2 addition, resulting in relatively more ether cleavage (A). Alternatively, an alternative C_β-O' ether cleavage pathway may exist after O_2 addition. In that case, H-bonding to the VBG peroxyl radical may impair formation of TS 4 and, thereby, slow down VBG_{ox} formation, resulting in relatively more ether cleavage (B). Based on the pK_a equalization principle,[33] it is expected that citrate^{3-} and HPO_4^{2-} can form reasonably strong hydrogen bonds with the secondary alcohol proton. It should be noted that, also in scenario A, the hydroperoxyl radical is expected to only be split off from a non-H-bonding peroxyl intermediate. Nevertheless, as O_2 addition is irreversible, the competition between ether cleavage and C_α-oxidation in scenario A is not dependent on the rate of hydroperoxyl split-off, but purely governed by the rates of ether cleavage and O_2 addition. HBacc = hydrogen bond acceptor.

The second possibility is that the competition between C_β-O' ether cleavage and C_α-oxidation takes place after the addition of O_2. Although pathway C was shown to be implausible, it could be speculated that there is an alternative and more favorable ether cleavage pathway, starting from the peroxyl intermediate (structure 3 in Figure 8). If that is the case, it is highly conceivable that H-bonding between buffer anions and structure 3 would affect the competition, in favor of ether cleavage. As the second step of pathway A involves an intramolecular H-transfer (TS 4 in Figure 8), strong H-bonding of the secondary alcohol proton to buffer anions would slow down this reaction step by impairing the formation of TS 4 (Figure 10B). Valgimigli et al. reported previously that the rate of a comparable reaction is, indeed, decreased by H-bond formation between substrate and solvent.[36] Whether an alternative and favorable ether cleavage pathway exists after O_2 addition remains to be investigated.

CONCLUSIONS

In conclusion, we have shown that the competition between ether cleavage and C_α-oxidation of a nonphenolic β-O-4′ linked lignin model in LMS incubations is highly dependent on

https://dx.doi.org/10.1021/acscatal.0c02154
ACS Catal. 2020, 10, 8650−8659

the reaction conditions. Both the relative and absolute extent of ether cleavage can be dramatically enhanced by increasing buffer pH and buffer strength. Furthermore, based on both experimental and computational efforts, we have provided new insights into the reaction mechanisms underlying C_α-oxidation and ether cleavage, and proposed that increased H-bonding between buffer anions and the C_α−OH group of the lignin model structure drives the outcome of LMS treatment toward ether bond cleavage. We expect that these insights will be useful in further studies and optimizations of oxidative lignin degradation in industrial settings. Our results showed that laccase-induced degradation of HBT was substantially lower at increased buffer strength and pH. Nonetheless, as still a significant portion of HBT was degraded, future research should focus on finding more stable mediating compounds that can be used at lower concentrations.

■ ASSOCIATED CONTENT

Supporting Information

The Supporting Information is available free of charge at https://pubs.acs.org/doi/10.1021/acscatal.0c02154.

Background information on H-bonding, additional RP-UHPLC-PDA-MS data, 2D NMR spectra, oxygen consumption measurement, laccase and HBT recovery after incubation, and optimized geometry and Cartesian coordinates of TS 2 (PDF)

■ AUTHOR INFORMATION

Corresponding Author

Mirjam A. Kabel − *Laboratory of Food Chemistry, Wageningen University and Research, 6708 WG Wageningen, The Netherlands;* orcid.org/0000-0002-1544-1744; Phone: +31 (0)317 483209; Email: mirjam.kabel@wur.nl

Authors

Roelant Hilgers − *Laboratory of Food Chemistry, Wageningen University and Research, 6708 WG Wageningen, The Netherlands;* orcid.org/0000-0002-3410-8795

Annemieke van Dam − *Laboratory of Organic Chemistry, Wageningen University and Research, 6708 WE Wageningen, The Netherlands*

Han Zuilhof − *Laboratory of Organic Chemistry, Wageningen University and Research, 6708 WE Wageningen, The Netherlands; School of Pharmaceutical Sciences and Technology, Tianjin University, 300072 Tianjin, China*

Jean-Paul Vincken − *Laboratory of Food Chemistry, Wageningen University and Research, 6708 WG Wageningen, The Netherlands;* orcid.org/0000-0001-8540-4327

Complete contact information is available at: https://pubs.acs.org/10.1021/acscatal.0c02154

Notes

The authors declare no competing financial interest.

■ ACKNOWLEDGMENTS

Dr. Pieter de Waard (MAGNEFY, Wageningen UR) is greatly acknowledged for performing the NMR analyses.

■ REFERENCES

(1) Munk, L.; Sitarz, A. K.; Kalyani, D. C.; Mikkelsen, J. D.; Meyer, A. S. Can laccases catalyze bond cleavage in lignin? *Biotechnol. Adv.* **2015**, *33* (1), 13−24.

(2) Lundquist, K.; Parkås, J. Different types of phenolic units in lignins. *BioResources* **2011**, *6* (2), 920−926.

(3) Rodriguez Couto, S.; Toca Herrera, J. L. Industrial and biotechnological applications of laccases: a review. *Biotechnol. Adv.* **2006**, *24* (5), 500−513.

(4) d'Acunzo, F.; Baiocco, P.; Fabbrini, M.; Galli, C.; Gentili, P. A mechanistic survey of the oxidation of alcohols and ethers with the enzyme laccase and its mediation by TEMPO. *Eur. J. Org. Chem.* **2002**, *2002* (24), 4195−4201.

(5) Baiocco, P.; Barreca, A. M.; Fabbrini, M.; Galli, C.; Gentili, P. Promoting laccase activity towards non-phenolic substrates: a mechanistic investigation with some laccase−mediator systems. *Org. Biomol. Chem.* **2003**, *1* (1), 191−197.

(6) d'Acunzo, F.; Baiocco, P.; Galli, C. A study of the oxidation of ethers with the enzyme laccase under mediation by two N−OH−type compounds. *New J. Chem.* **2003**, *27* (2), 329−332.

(7) Kawai, S.; Nakagawa, M.; Ohashi, H. Degradation mechanisms of a nonphenolic *β-O*-4 lignin model dimer by *Trametes versicolor* laccase in the presence of 1-hydroxybenzotriazole. *Enzyme Microb. Technol.* **2002**, *30* (4), 482−489.

(8) Kawai, S.; Umezawa, T.; Shimada, M.; Higuchi, T. Aromatic ring cleavage of 4,6-di-(tert-butyl)-guaiacol, a phenolic lignin model compound, by laccase of *Coriolus versicolor*. *FEBS Lett.* **1988**, *236* (2), 309−311.

(9) Kawai, S.; Nakagawa, M.; Ohashi, H. Aromatic ring cleavage of a non-phenolic *β-O*-4 lignin model dimer by laccase of *Trametes versicolor* in the presence of 1-hydroxybenzotriazole. *FEBS Lett.* **1999**, *446* (2−3), 355−358.

(10) Kawai, S.; Umezawa, T.; Higuchi, T. Degradation mechanisms of phenolic *β*-1 lignin substructure model compounds by laccase of *Coriolus versicolor*. *Arch. Biochem. Biophys.* **1988**, *262* (1), 99−110.

(11) Kawai, S.; Asukai, M.; Ohya, N.; Okita, K.; Ito, T.; Ohashi, H. Degradation of a non-phenolic *β-O*-4 substructure and of polymeric lignin model compounds by laccase of *Coriolus versicolor* in the presence of 1-hydroxybenzotriazole. *FEMS Microbiol. Lett.* **1999**, *170* (1), 51−57.

(12) Srebotnik, E.; Hammel, K. E. Degradation of nonphenolic lignin by the laccase/1-hydroxybenzotriazole system. *J. Biotechnol.* **2000**, *81* (2), 179−188.

(13) Although ether cleavage may eventually also result in the formation of ketone groups at the C_α-position, in this paper the term C_α-oxidation is used to describe the conversion of C_α-OH to a C_α=O without concomitant ether cleavage.

(14) Heap, L.; Green, A.; Brown, D.; van Dongen, B.; Turner, N. Role of laccase as an enzymatic pretreatment method to improve lignocellulosic saccharification. *Catal. Sci. Technol.* **2014**, *4* (8), 2251−2259.

(15) Hilgers, R.; Twentyman-Jones, M.; van Dam, A.; Gruppen, H.; Zuilhof, H.; Kabel, M. A.; Vincken, J.-P. The impact of lignin sulfonation on its reactivity with laccase and laccase/HBT. *Catal. Sci. Technol.* **2019**, *9* (6), 1535−1542.

(16) Li, K.; Xu, F.; Eriksson, K.-E. L. Comparison of fungal laccases and redox mediators in oxidation of a nonphenolic lignin model compound. *Appl. Environ. Microbiol.* **1999**, *65* (6), 2654−2660.

(17) Fabbrini, M.; Galli, C.; Gentili, P. Comparing the catalytic efficiency of some mediators of laccase. *J. Mol. Catal. B: Enzym.* **2002**, *16* (5), 231−240.

(18) Moldes, D.; Díaz, M.; Tzanov, T.; Vidal, T. Comparative study of the efficiency of synthetic and natural mediators in laccase-assisted bleaching of Eucalyptus kraft pulp. *Bioresour. Technol.* **2008**, *99* (17), 7959−7965.

(19) Ibarra, D.; Romero, J.; Martínez, M. J.; Martínez, A. T.; Camarero, S. Exploring the enzymatic parameters for optimal delignification of Eucalypt pulp by laccase-mediator. *Enzyme Microb. Technol.* **2006**, *39* (6), 1319−1327.

(20) Barreca, A. M.; Fabbrini, M.; Galli, C.; Gentili, P.; Ljunggren, S. Laccase/mediated oxidation of a lignin model for improved delignification procedures. *J. Mol. Catal. B: Enzym.* **2003**, *26* (1−2), 105−110.

(21) Hilgers, R. J.; Vincken, J.-P.; Gruppen, H.; Kabel, M. A. Laccase/mediator systems: Their reactivity towards phenolic lignin structures. *ACS Sustainable Chem. Eng.* **2018**, *6* (2), 2037−2046.
(22) Frisch, M. J.; et al. *Gaussian 16*, revision B. 01; Gaussian Inc.: Wallingford, CT, 2016.
(23) Shleev, S.; Persson, P.; Shumakovich, G.; Mazhugo, Y.; Yaropolov, A.; Ruzgas, T.; Gorton, L. Interaction of fungal laccases and laccase-mediator systems with lignin. *Enzyme Microb. Technol.* **2006**, *39* (4), 841−847.
(24) Camarero, S.; Ibarra, D.; Martínez, Á. T.; Romero, J.; Gutiérrez, A.; Del Río, J. C. Paper pulp delignification using laccase and natural mediators. *Enzyme Microb. Technol.* **2007**, *40* (5), 1264−1271.
(25) Gutiérrez, A.; Rencoret, J.; Cadena, E. M.; Rico, A.; Barth, D.; Del Río, J. C.; Martínez, Á. T. Demonstration of laccase-based removal of lignin from wood and non-wood plant feedstocks. *Bioresour. Technol.* **2012**, *119*, 114−122.
(26) Rencoret, J.; Pereira, A.; Del Río, J. C.; Martínez, A. T.; Gutiérrez, A. Laccase-mediator pretreatment of wheat straw degrades lignin and improves saccharification. *BioEnergy Res.* **2016**, *9* (3), 917−930.
(27) Kawai, S.; Iwatsuki, M.; Nakagawa, M.; Inagaki, M.; Hamabe, A.; Ohashi, H. An alternative β-ether cleavage pathway for a non-phenolic β-*O*-4 lignin model dimer catalyzed by a laccase-mediator system. *Enzyme Microb. Technol.* **2004**, *35* (2−3), 154−160.
(28) d'Acunzo, F.; Baiocco, P.; Fabbrini, M.; Galli, C.; Gentili, P. The radical rate-determining step in the oxidation of benzyl alcohols by two N−OH-type mediators of laccase: the polar N-oxyl radical intermediate. *New J. Chem.* **2002**, *26* (12), 1791−1794.
(29) Melander, L.; Saunders, W. *Reaction rates of isotopic molecules*; Wiley: New York, 1980.
(30) Ten Have, R.; Teunissen, P. J. M. Oxidative mechanisms involved in lignin degradation by white-rot fungi. *Chem. Rev.* **2001**, *101* (11), 3397−3414.
(31) Clayden, J.; Greeves, N.; Warren, S.; Wothers, P. *Organic Chemistry*, 2nd ed.; Oxford University Press, 2012; p 240.
(32) GENG, M.; DUAN, Z. Prediction of oxygen solubility in pure water and brines up to high temperatures and pressures. *Geochim. Cosmochim. Acta* **2010**, *74* (19), 5631−5640.
(33) Gilli, P.; Pretto, L.; Bertolasi, V.; Gilli, G. Predicting hydrogen-bond strengths from acid-base molecular properties. The pKa slide rule: toward the solution of a long-lasting problem. *Acc. Chem. Res.* **2009**, *42* (1), 33−44.
(34) Bejan, E. V.; Font-Sanchis, E.; Scaiano, J. C. Lactone-derived carbon-centered radicals: formation and reactivity with oxygen. *Org. Lett.* **2001**, *3* (25), 4059−4062.
(35) Wright, J. S.; Shadnia, H.; Chepelev, L. L. Stability of carbon-centered radicals: effect of functional groups on the energetics of addition of molecular oxygen. *J. Comput. Chem.* **2009**, *30* (7), 1016−1026.
(36) Valgimigli, L.; Amorati, R.; Fumo, M. G.; DiLabio, G. A.; Pedulli, G. F.; Ingold, K. U.; Pratt, D. A. The unusual reaction of semiquinone radicals with molecular oxygen. *J. Org. Chem.* **2008**, *73* (5), 1830−1841.

https://dx.doi.org/10.1021/acscatal.0c02154
ACS Catal. 2020, 10, 8650−8659